

Journal of Biomedical Optics

SPIEDigitalLibrary.org/jbo

***In vivo* dynamic process imaging using real-time optical-resolution photoacoustic microscopy**

Wei Shi
Peng Shao
Parsin Hajireza
Alexander Forbrich
Roger J. Zemp

In vivo dynamic process imaging using real-time optical-resolution photoacoustic microscopy

Wei Shi, Peng Shao, Parsin Hajireza, Alexander Forbrich, and Roger J. Zemp

University of Alberta, Department of Electrical and Computer Engineering, Edmonton, Alberta, Canada, T6G 2V4

Abstract. The authors demonstrate *in vivo* dynamic process imaging using a label-free real-time optical-resolution photoacoustic microscope (OR-PAM). This reflection-mode system takes advantage of a 532-nm fiber laser source with a high pulse repetition rate of up to 600 kHz combined with a fast-scanning mirror system. Microvasculature in SCID mouse ears is imaged at near real-time (0.5 fps) for a 1×1 mm² field of view (FOV) with micron-scale lateral resolution. We also demonstrate imaging of cardiac-induced microhemodynamics in murine microvasculature at real-time frame-rates (30 fps) over a 250×250 μm^2 FOV using real-time C-scan OR-PAM with ability to provide sustained imaging with near real-time feedback for focusing and positioning. © The Authors. Published by SPIE under a Creative Commons Attribution 3.0 Unported License. Distribution or reproduction of this work in whole or in part requires full attribution of the original publication, including its DOI. [DOI: [10.1117/1.JBO.18.2.026001](https://doi.org/10.1117/1.JBO.18.2.026001)]

Keywords: photoacoustic microscopy; fiber laser.

Paper 12546P received Aug. 21, 2012; revised manuscript received Dec. 20, 2012; accepted for publication Jan. 2, 2013; published online Feb. 1, 2013.

1 Introduction

Optical-resolution photoacoustic microscopy (OR-PAM) is an emerging imaging technology with high lateral resolution due to tightly focused micron-scale laser spot size, and high contrast in tissue based on optical absorption. Maslov et al.,¹ first demonstrated *in vivo* imaging of the microvasculature including single capillaries in mice using OR-PAM with a lateral resolution of 5 μm at imaging depths >0.7 mm. Later, more studies on using novel OR-PAM techniques for structural² and functional²⁻⁶ imaging were reported. OR-PAM has demonstrated its potential applications for neuro-functional imaging, oxygen saturation imaging,^{3,4} blood velocity imaging,⁵ and transcranial imaging of whole brain murine cortical capillary networks.⁶ In addition, OR-PAM was reported to realize *in vivo* imaging of amyloid plaques in a transgenic mouse model of Alzheimer's disease,⁷ as well as longitudinal monitoring of angiogenesis in a transgenic mouse model,^{8,9} demonstrating the potential to monitor the efficacy of anti-angiogenic therapies.

In order to extend the applications of OR-PAM to clinical applications, ease of use and real-time operation will be key factors to be implemented. Both laser pulse repetition rate (PRR) and scanning speed are important factors affecting the imaging speed. Recently, Hu et al.¹⁰ developed a second-generation OR-PAM system based on mechanical translation of an imaging head. They reported a 70-min image acquisition time for a 7.8×10 mm² FOV with a pixel size of 2.5×2.5 μm^2 . Translating the imaging head instead of the living object accelerated the scanning speed by a factor of five.¹⁰ However, despite high image quality, imaging speed was far below real-time rates. Xie et al.¹¹ reported a laser-scanning OR-PAM with only laser light being raster scanned by an $x-y$ galvanometer mirror system while keeping the ultrasonic transducer stationary. The system enabled fast scanning speed but with imaging speed limited

mainly by their kHz PRR laser. In 2010, our group demonstrated laser-scanning

OR-PAM imaging using passively Q-switched microchip lasers with PRR exceeding 10 kHz and fiber lasers with 100 kHz PRR.¹² Later, a 50 kHz fiber-laser operating at 1064 nm for OR-PAM is reported by Wang et al.¹³ In 2011, our group demonstrated an OR-PAM system using a fiber laser source with high repetition rate of up to 600 kHz capable of C-scan imaging at four frames per second.¹⁴ However, the system was limited to acquisition of only two to three volumetric datasets due to memory limitations, and sustained real-time imaging was not possible. Rao et al.¹⁵ reported a high-speed OR-PAM system in an inverted microscope configuration with Au nanoparticle-assisted sub-diffraction-limit resolution. With a 100 kHz pulsed laser, a stationary ultrasonic transducer and a two-dimensional (2-D)-Galvo system scanning the collimated laser beam through the pupil of objective lens, their system demonstrated its ability to achieve *in vivo* imaging of microcirculation in mouse skin at 18 three-dimensional volumes per second with repeated 2-D raster scans of 100 by 50 points for 100×50 μm^2 image size with 0.23 μm point size and 256 A-line measurements at each points. However, their setup worked only in transmission mode, which limits its applications for thick soft tissue. Also, imaging microcirculation in their system required the assistance of nanoparticle agents. In Ref. 16, a second generation OR-PAM system was used to acquire ECG-gated measurements of blood pulse-waves in small vessels. This novel approach offered outstanding image quality and provided for the first time estimates of pulse-wave velocities using photoacoustic imaging; however, real-time C-scan visualization was not possible. Yao et al.¹⁷ demonstrated an immersible MEMS-mirror scanning system capable of high volumetric frame rates and imaging of carbon particles and red blood cells; however, they did not correlate microvascular hemodynamics with cardiac pulsations, which could be important in pulse-wave velocity studies. In our previous studies,¹⁴ we were not able to image dynamic processes due to previous data acquisition limitations of our system. In this paper, we demonstrate an improved fast C-scan OR-PAM

Address all correspondence to: Roger J. Zemp, University of Alberta, Department of Electrical and Computer Engineering, Edmonton, Alberta, Canada, T6G 2V4. Tel: 1-780-492-1825; Fax: 1-780-492-1811; E-mail: rzemp@ualberta.ca

system, which enables both sustained imaging and real-time imaging. We report *in vivo* label-free reflection-mode real-time OR-PAM imaging of micro-hemodynamics correlated with cardiac pulsations and anticipate this system can play an important role in future functional imaging studies of neural-hemodynamic coupling.

2 Methods

Figure 1 shows the schematic of the real-time OR-PAM system. Laser pulses with high repetition rate ranging from 20 kHz to 600 kHz are generated by a diode-pumped pulsed Ytterbium-doped fiber laser (GLP-10, IPG Photonics Corporation.). Via a built-in compact laser head, the 1064-nm fundamental wavelength is frequency-doubled to 532-nm and is then collimated for free space output. Laser amplifier pump power can be adjusted to provide nanosecond laser pulses with programmable pulse energy up to 20 μ J. A small amount of light is reflected by a glass slide onto a high speed custom photodiode to generate trigger signals for a data acquisition card (PCI 6221, National Instruments Corporation). A 2-D galvanometer scanning mirror system (6230H, Cambridge Technology Inc.) deflected the incident laser beam onto an 18-mm-focal-length objective lens positioned \sim 3.6 cm below. With 2-D XY mirrors driven by analog sinusoidal signals from a dual channel function generator (AFG3022B Tektronix Inc.), the raster scanning of the laser beam on the objective lens focal plane was realized. The scanning angles are determined by the amplitudes of the sinusoidal signals outputs from the function generator. Together with the focal length of objective lens, the maximum scanning angles on both axes determine the image FOV. Also, the maximum scanning angles limit the maximum scanning speed that the mirrors can reach up to several kHz for small angles. The laser beam scanned onto the objective lens is focused through our unique light-delivery probe adapted from our previous work.^{12,14,18} As shown in Fig. 1, a downfacing 10-mm silica prism together with optical index-matching fluid (Catalog No. 19569, Cargille Labs, Cedar, Grove, New Jersey) and a thin transparent plastic membrane to hold the index-fluid in place enabled a top-down laser beam to be directed to the object without optical refractive path

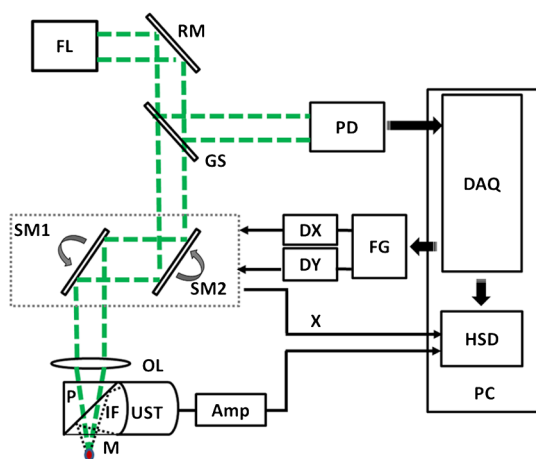


Fig. 1 Experiment setup of the real-time OR-PAM system (FL: fiber laser; RM: high reflectivity mirror; GS: glass slide; PD: photodiode; SM1, SM2: scanning mirror; DX, DY: galvanometer scanning mirror driver; FG: 2-channel function generator; DAQ: data acquisition card; OL: 18-mm objective lens; P: prism; IF: index-matching fluid; M: membrane; UST: ultrasonic transducer; Amp: amplifier; HSD: high speed digitizer).

deviation. The object is positioned underneath the membrane at the focal plane of both the objective lens and a 3.5 MHz focused ultrasound transducer (19-mm focus, 6-mm active element, $f = 3.17$, CD International Inc.). The generated upwards photoacoustic signal was reflected by the optical prism and then received by the ultrasound transducer. According to our previous work,¹⁸ acoustic attenuation in the index matching fluid is measured to be only slightly higher than that in water. Also, for acoustic signal within the angular acceptance of the transducer, the acoustic reflectivity on the prism and index matching fluid interface is almost 100%.¹⁸

Two data acquisition methods were developed on the system configured in Fig. 1: long acquisition mode and multiple-record acquisition mode. In long acquisition mode, for each frame, the system collects photoacoustic signals from a large number of laser shots in one long acquisition and then block-transfers data to the PC random-access memory (RAM). With this method, data acquisition time is based on both the data collection time and data block-transferring time. The fast (\sim 200 MB/s) data block-transfer rate capabilities of the high speed digitizer (CS8289, Gage Cobra, Gage Applied Systems, Inc.) enable sustained data acquisition. High frame rate is achievable for small FOV where data block-transfer time is short due to the small amount of data needing to be transferred. In multiple-record acquisition mode, the system collects photoacoustic signals for each laser shot in one acquisition and transfers data when all data collection is done. With this method, high frame rate is achievable since there is no data transfer time between acquisition records. However, transfer of all data collection at the end requires substantially longer time than transfer of a large single acquisition data in long acquisition mode. Therefore, sustained real-time acquisition is difficult to realize in this method. Nevertheless, it can be used to realize real-time imaging for a small FOV with limited number of frame acquisitions limited by memory buffer size of 128 MB. Its real-time nature can be used for imaging of microcirculation hemodynamics.

3 Results

The OR-PAM system is utilized for imaging *in vivo* dynamic processes. Seven-week old SCID Hairless Outbred (SHOTM, Charles River, Massachusetts, USA) mice were used for our *in vivo* imaging studies. The animals were anesthetized using a breathing anesthesia system (E-Z Anesthesia, Euthanex Corp.) during image acquisition. All experimental animal procedures were conducted in conformity with the laboratory animal protocol approved by the Animal Use and Care Committee of the University of Alberta.

Animal imaging experiments demonstrated the dynamic imaging capability of our system. During the experiments, the diode-pumped pulsed Ytterbium-doped fiber laser generated 320 kHz, \sim 1 ns, 532-nm laser pulses with \sim 0.1 μ J (measured after the objective lens). The raster scanning frequencies on two axes were set as 1 Hz on the Y axis and 400 Hz on the X axis, and both maximum optical scanning angles were \sim 1.6 deg, which corresponds to 1×1 mm² FOV. A high-precision motorized translation stage (not shown in Fig. 1) was used to translate the mice each time after one frame scan was finished. The position of the stage was sensed by encoders and recorded. The long acquisition mode technique was used for sustained imaging of translations. For the repeated 2-D scans of 400 by 400 points with 156 A-line measures at each point, the photoacoustic

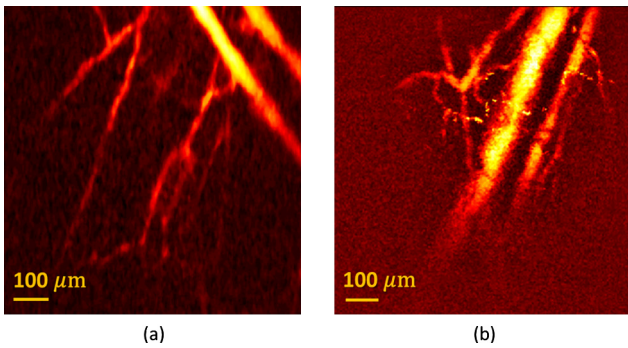


Fig. 2 (a) An *in vivo* image of micro-vasculatures obtained from a hairless SCID mouse ear to demonstrate the imaging capability of our imaging system; (b) A snapshot from the *in vivo* movie composed of 41 frame $1 \text{ mm} \times 1 \text{ mm}$ images of microvasculature in an SCID hairless mouse ear when the mouse was in a vertical movement; (Video 1, MPEG, 4.0 MB) [URL: <http://dx.doi.org/10.1117/1.JBO.18.2.026001.1>] displays at 2 fps while the actual system frame rate is about 0.5 fps; some small capillaries come out and disappear during the vertical translation.

data collection time was 0.5 s. Block-data transfer time was a slightly over 0.5 s, resulting in a frame rate of 0.5 fps, which means 1D A-scan rate of 80,000 Hz. Figure 2(a) shows a maximum-amplitude-projection (MAP) snapshot of microvasculature in an SCID mouse ear to demonstrate the imaging capability of our system. It clearly depicts the vessels including small capillaries. This is consistent with previous resolution studies using our OR-PAM system with $\sim 6\text{-}\mu\text{m}$ resolution.^{12,14} Figure 2(b) shows a snapshot taken from a movie of microvasculature MAP images in an SCID mouse ear as well but with the mouse under $6 \mu\text{m}$ per step vertical translation for focusing. Vessels including capillaries are visualized. The corresponding movie is displayed at 2 fps in Video 1. It includes a total of 41-frame $1 \times 1 \text{ mm}^2$ images acquired at 0.5 fps. Some small capillaries show up and disappear in the video as the mouse is translated.

In our studies on imaging dynamic processes of micro-hemodynamics, the diode-pumped pulsed Ytterbium-doped fiber laser generated 300-kHz, $\sim 1\text{-ns}$, 532-nm laser pulses with $\sim 0.1 \mu\text{J}$. Raster scanning frequencies of the fast-scanning mirrors were set as 15 Hz for the *Y* axis and 1.5 kHz for the *X* axis. Therefore, the data collection rate can reach 30 fps (two

times the slow axis scan rate). Also, due to the limitation of the scanning galvanometer mirror system, the maximum optical scanning angles of both mirrors are set as ~ 0.4 deg. The resulting imaging area was $250 \times 250 \mu\text{m}^2$. The mice were kept stationary during the experiment. Multirecord acquisition mode was adapted as the data acquisition method to reach a frame-rate of 30 fps over a limited number of frame acquisitions with 156 A-line measures at each point for 100 by 100 repeated 2-D scans. The corresponding 1D A-scan rate was 300,000 Hz. Figure 3(a) shows a single frame from a movie representing MAP images of microvasculature in an SCID mouse ear. The corresponding movie (Video 2) is composed of 42-frame $250 \times 250 \mu\text{m}^2$ images taken at a frame rate of 30 fps. A periodic variation in photoacoustic intensity was observed, which we hypothesize is the flow of blood cells through the vessels due to cardiac cycle-induced pulse waves propagating through arterioles. We examined the photoacoustic signal amplitude over time within the dashed box region A indicated in Fig. 3(a) by averaging the intensity as seen in Fig. 3(b). The intensity variation is about 35% with ~ 5 peaks clearly depicted in ~ 1.4 s, which is consistent with the heart rate of an anaesthetized mouse measured independently by a pulse-oximeter. For comparison, we examined the photoacoustic signal amplitude over time within the dashed box region B and C indicated in Fig. 3(a) respectively, while region C did not include visible blood vessels. The intensity variation for B is similar to that of A, while the intensity variation for C is within 5%, much less compared with studies on region A and B. In addition, the pulse energy instability of the diode-pumped pulsed Ytterbium-doped fiber laser used here is within 1%.

4 Discussion

In vivo images of microvasculature in SCID mouse ears under translations, with an average pixel separation of $2.5 \mu\text{m}$ within an FOV of $1 \times 1 \text{ mm}^2$, were obtained at a frame-rate of 0.5 fps. Higher frame rate with sustained imaging is achievable for smaller FOV (~ 7 fps for a FOV of $250 \times 250 \mu\text{m}$). The step size for the vertical translation in Fig. 2 is $6 \mu\text{m}$. So for 41 frames, it moved $\sim 240 \mu\text{m}$ in total. Some small vessels including capillaries are seen to come into and out of focus with vertical translation. However, this is less evident for larger vessels. One explanation of this is that for targets larger than the spot size, with OR-PAM (which, like conventional microscopy uses one-way focusing) the photoacoustic axial depth of field

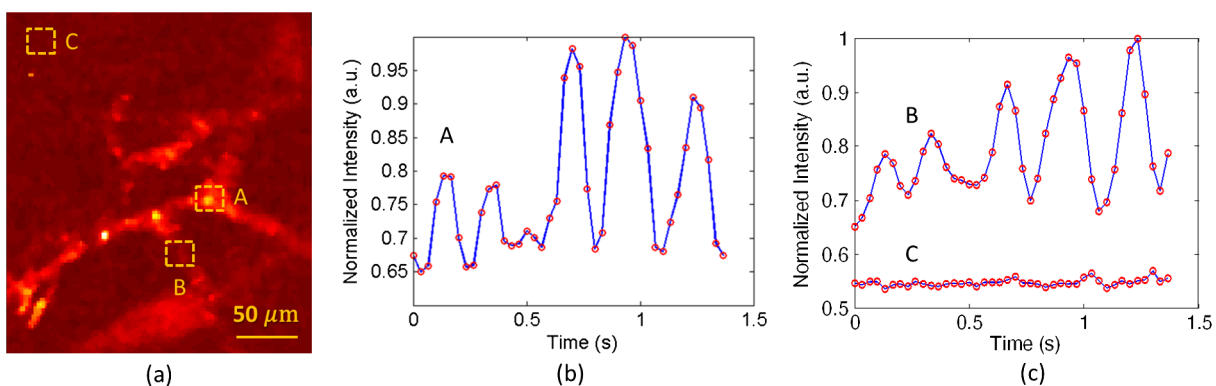


Fig. 3 (a) A snapshot from the *in vivo* movie composed of 42 frame $250 \times 250 \mu\text{m}^2$ images of microvasculature in an SCID hairless mouse ear acquired at 30 fps; (Video 2, MPEG, 412 KB) [URL: <http://dx.doi.org/10.1117/1.JBO.18.2.026001.2>] displays at 15 fps, while microvasculature motions and blood intensity changes are clear to see. (b) Mean photoacoustic signal amplitude inside the dash box A indicated area in (a) versus time. (c) Mean photoacoustic signal amplitude inside the dash box B and C indicated area in (a) respectively versus time.

is effectively much larger than the optical depth of field of the focused beam (estimated as $\sim 35 \mu\text{m}$).¹⁹ This, coupled with poor axial resolution ($\sim 500 \mu\text{m}$) leads to lack of clear axial focusing/defocusing for large targets. The sustained high resolution fast imaging demonstrated the capability of our system to be used for real-time focusing and positioning. Near real-time positioning will permit panning over large areas with mm FOV windows and then locating regions of interest for further studies.

Video 2 is the label-free reflection-mode OR-PAM demonstration of imaging micro-hemodynamics. One observation, already noted, is the intensity variations that correlate with cardiac cycle. This may in part be explained by surges of blood periodically surging through arterioles due to cardiac-induced pulse-waves. Another observation is that some vascular branches seem to have negligible flow then seemingly random transient surges. These effects deserve additional study and could be due to microhemodynamic regulatory mechanisms. The effects seen can be discounted as artifacts, however, because laser pulse-to-pulse intensity variation is less than 1% and scanning of stationary phantom structures shows no motion. It is noteworthy to point out that optical coherence tomography can provide excellent structural images of microvasculature.^{20,21} However, to date, these systems have not been able to provide video-rate imaging of comparable tissue volumes due to the necessity of requiring multiple A-scan lines to extract motion of scatterers. Intravital microscopy is a powerful technique that has been capable of studying microhemodynamics.²² However, this technique requires surgical exposure of thin transparent membranes and is not suitable for noninvasive reflection-mode imaging.

The unique capabilities of our system may prove important for imaging cortical hemodynamics in functional brain mapping studies. Real-time focusing and positioning should facilitate translation of the technique to clinical settings. While FOV is limited in our real-time scanning, mosaicing of small patches should provide larger-FOV images, as described by our recent work.²³

For 2-D laser scanning OR-PAM systems using a focused transducer, the FOV is limited by the focal width of the ultrasonic transducer. Therefore, we used a low frequency (3.5 MHz) ultrasonic transducer to achieve a large FOV. The axial resolution of the 3.5 MHz ultrasonic transducer can be calculated as near $500 \mu\text{m}$, sacrifice of axial resolution is tolerable for MAP images. A future design could match the receiver bandwidth to the bandwidth of the high-frequency photoacoustic signals to improve signal-noise-ratio (SNR) at the expense of FOV.

In our *in vivo* studies, given that the optical focus is $\sim 150 \mu\text{m}$ beneath the tissue surface, with an objective lens NA of 0.15, the surface spot size is $\sim 45 \mu\text{m}$ in diameter, and the calculated surface laser fluence is $\sim 5 \text{ mJ}/\text{cm}^2$, below the single pulse limit of $20 \text{ mJ}/\text{cm}^2$ set by the American National Standards Institute (ANSI).²⁴ The spatial peak optical fluence at the focus in water is $\sim 500 \text{ mJ}/\text{cm}^2$, which is still less than the damage threshold observed in small animals.²⁵ In our work, light delivery is confined to a localized area, and no tissue damage is visible after imaging.

In addition, for an average pixel separation of $2.5 \mu\text{m}$, there are on average $N = 45 \mu\text{m}/2.5 \mu\text{m} \sim 18$ adjacent laser pulses overlapping on the skin surface. For 320 kHz laser PRR, the exposure time is $t \sim 56 \mu\text{s}$, so the MPE for a pulse train is $\text{MPE}_{\text{Train}} = 1.1 C_A t^{0.25} = 95 \text{ mJ}/\text{cm}^2$, where C_A is a wavelength-correction factor equal to unity for 400 to 700 nm wavelengths. The average power limit set by ANSI is calculated as

$\text{MPE}_{\text{Average}} = \text{MPE}_{\text{Train}}/N \sim 5 \text{ mJ}/\text{cm}^2$, which is our estimated fluence per pulse at the skin surface. This means that we are essentially at our theoretical upper limit for pulse-repetition rate; however, the repetition rate could be increased if pulse-energy can be lowered and SNR improved. In future studies, careful selection of focusing, repetition rate, and pulse energy parameters must be considered to avoid exceeding ANSI limits. On the other hand, for some preclinical applications, exceeding these limits may be acceptable.

5 Conclusion

We have demonstrated an OR-PAM system capable of near real-time sustained imaging to aid focusing and positioning, and a real-time frame-limited mode capable of imaging micro-circulation pulsatile hemodynamics. This OR-PAM system enabled label-free reflection-mode imaging of micro-hemodynamics at real-time rates. The fast acquisition capabilities of the system may pave the way for clinical adaptation and preclinical studies such as functional brain imaging.

Acknowledgments

We gratefully acknowledge funding from NSERC (355544-2008, 375340-2009, STPGP 396444), Terry-Fox Foundation and the Canadian Cancer Society (TFF 019237, TFF 019240, CCS 2011-700718), the Alberta Cancer Research Institute (ACB 23728), the Canada Foundation for Innovation, Leaders Opportunity Fund (18472), Alberta Advanced Education & Technology, Small Equipment Grants Program (URSI09007SEG), Microsystems Technology Research Initiative (MSTRI RES0003166), University of Alberta Startup Funds, Alberta Ingenuity/Alberta Innovates scholarships for graduate and undergraduate students, and Canadian Federation of University Women Edmonton Margaret Brine Graduate Scholarships for Women.

References

1. K. Maslov et al., "Optical-resolution photoacoustic microscopy for *in vivo* imaging of single capillaries," *Opt. Lett.* **33**(9), 929–931 (2008).
2. S. Hu, K. Maslov, and L. V. Wang, "Noninvasive label-free imaging of microhemodynamics by optical-resolution photoacoustic microscopy," *Opt. Express* **17**(9), 7688–7693 (2009).
3. S. Hu, K. Maslov, and L. V. Wang, "*In vivo* functional chronic imaging of a small animal model using optical-resolution photoacoustic microscopy," *Med. Phys.* **36**(6), 2320–2323 (2009).
4. L. Song, K. Maslov, and L. V. Wang, "Multifocal optical-resolution photoacoustic microscopy *in vivo*," *Opt. Lett.* **36**(7), 1236–1237 (2011).
5. J. Yao et al., "*In vivo* photoacoustic imaging of transverse blood flow using Doppler broadening of bandwidth," *Opt. Lett.* **35**(9), 1419–1421 (2010).
6. S. Hu et al., "Functional transcranial brain imaging by optical-resolution photoacoustic microscopy," *J. Biomed. Opt.* **14**(4), 040503 (2009).
7. S. Hu et al., "Intravital imaging of amyloid plaques in a transgenic mouse model using optical-resolution photoacoustic microscopy," *Opt. Lett.* **34**(24), 3899–3901 (2009).
8. S. Oladipupo et al., "Conditional HIF-1 induction produces multistage neovascularization with stage-specific sensitivity to VEGFR inhibitors and myeloid cell independence," *Blood* **117**(15), 4142–4153 (2011).
9. S. Oladipupo et al., "VEGF is essential for hypoxia-inducible factor mediated neovascularization but dispensable for endothelial sprouting," *PNAS* **108**(32), 13264–13269 (2011).
10. S. Hu, K. Maslov, and L. V. Wang, "Second-generation optical-resolution photoacoustic microscopy with improved sensitivity and speed," *Opt. Lett.* **36**(7), 1134–1136 (2011).
11. Z. X. Xie et al., "Laser-scanning optical-resolution photoacoustic microscopy," *Opt. Lett.* **34**(12), 1771–1773 (2009).

12. W. Shi et al., "Optical resolution photoacoustic microscopy using novel high-repetition-rate passively Q-switched microchip and fiber lasers," *J. Biomed. Opt.* **15**(5), 056017 (2010).
13. Y. Wang et al., "Fiber-laser-based photoacoustic microscopy and melanoma cell detection," *J. Biomed. Opt.* **16**(1), 011014 (2011).
14. W. Shi et al., "*In vivo* near-realtime volumetric optical-resolution photoacoustic microscopy using a high-repetition-rate nanosecond fiber-laser," *Opt. Express* **19**(18), 17143–17150 (2011).
15. B. Rao et al., "Real-time four-dimensional optical-resolution photoacoustic microscopy with Au nanoparticle-assisted subdiffraction-limit resolution," *Opt. Lett.* **36**(7), 1137–1139 (2011).
16. C. Yeh et al., "Photoacoustic microscopy of blood pulse wave," *J. Biomed. Opt.* **17**(7), 070504 (2012).
17. J. Yao et al., "Wide-field fast-scanning photoacoustic microscopy based on a water-immersible MEMS scanning mirror," *J. Biomed. Opt.* **17**(8), 080505 (2012).
18. J. C. Ranasinghesagara et al., "Photoacoustic technique for assessing optical scattering properties of turbid media," *J. Biomed. Opt.* **14**(4), 040504 (2009).
19. L. V. Wang and H. Wu, *Biomedical Optics: Principles and Imaging*, John Wiley & Sons Inc., Hoboken, New Jersey (2007).
20. A. Mariampillai et al., "Optimized speckle variance OCT imaging of microvasculature," *Opt. Lett.* **35**(8), 1257–1259 (2010).
21. G. Liu et al., "High-resolution imaging of microvasculature in human skin in-vivo with optical coherence tomography," *Opt. Express* **20**(7), 7694–7705 (2012).
22. A. M. Iga et al., "Quantitating therapeutic disruption of tumor blood flow with intravital video microscopy," *Cancer Res.* **66**(24), 11517–11519 (2006).
23. P. Shao et al., "Mosaicing acquisition and processing for optical resolution photoacoustic microscopy," *J. Biomed. Opt.* **17**(8), 080503 (2012).
24. Laser Institute of America, American National Standard for Safe Use of Lasers ANSI Z136.1-2007, American National Standards Institute, Inc. (2007).
25. V. P. Zharov et al., "*In vivo* photoacoustic flow cytometry formonitoring of circulating single cancer cells and contrast agents," *Opt. Lett.* **31**(24), 3623–3625 (2006).